Electronic Supplementary Information

An advanced cathode material for high-power Li-ion storage full cell with a long lifespan

Haijian Huang, [a] Long Pan, [a] Xi Chen, [a] Elena Tervoort, [a] Alla Sologubenko, [b] and Markus Niederberger*[a]

[a] Laboratory for Multifunctional Materials, Department of Materials, ETH Zürich, Vladimir-Prelog-Weg 5, 8093 Zürich, Switzerland.
E-mail: markus.niederberger@mat.ethz.ch

[b] Laboratory for Nanometallurgy, Department of Materials, ETH Zürich, Vladimir- Prelog-Weg 5, Zürich, 8093, Switzerland.

Experimental Section

Chemicals. Vanadium oxide (99.6+%, Acros Organics), nickel acetate tetrahydrate (99.998%, Aldrich), graphene oxide dispersion (5 mg mL^{-1} in H_2O, Royal Elite (Shanghai, China)), urea (99.0-100.5%, ABCR), acetone (>99.8%, Fisher Chemical), isopropanol (technical grade).

Synthesis of $Ni_{0.25}V_2O_5 \cdot nH_2O$ *(NVO).* Typically, Milli-Q water (18.8 mL, 18.2 MΩ·cm) was mixed with acetone (1.2 mL). Nickel acetate tetrahydrate (133 mg) and vanadium oxide (147 mg) were added to the above mixture, stirred for 10 min and then transferred to a microwave glass tube with an inner volume of 35 mL. The reaction mixture was heated to 210°C for 1 h in a CEM Hybrid microwave reactor. The resulting products were centrifuged, thoroughly rinsed with Milli-Q water and ~20 mL isopropanol, and finally dried in a vacuum oven at 80°C overnight.

Synthesis of NVO@rGO. For the synthesis of NVO@rGO, all the procedures were the same as those for NVO, except that the 8 mL Milli-Q water were substituted by the same amount of graphene oxide dispersion (5 mg mL^{-1} in H_2O).

Synthesis of the N-doped reduced graphene oxide (N-rGO) foam. The N-rGO foam was synthesized using methods adjusted from the literature.[1, 2] Typically, urea (10.8 g) was added to Milli-Q water (24.3 mL) and stirred until completely dissolved. The obtained solution was mixed with GO dispersion (7.2 mL, 5 mg mL^{-1} in water) under magnetic stirring. The mixture was transferred to a 45 ml Teflon container, sealed in a stainless-steel autoclave (Parr, Acid Digestion Vessel 4744) and heated in an oven at 180°C for 12 h. A gel-like monolith was obtained, which was thoroughly rinsed with water and freeze-dried on a Martin Christ freeze drier to obtain the final N-rGO foam monolith.

Characterization. X-ray diffraction (XRD) measurements were performed on a PANalytical Empyrean equipped with a Cu Kα X-ray tube (45 kV, 40 mA). The scanning electron microscopy (SEM) images were taken on a LEO 1530 Gemini. For transmission electron microscopy (TEM) observations, a FEI Talos F200X operated at 200kV and a JEOL JEM-1400 operated at 100kV were used. The scanning TEM (STEM) studies using an atomic number sensitive, high angle annular dark field (HAADF) mode were complemented by spectrum imaging (SI) using a SuperX EDX (energy-dispersive X-ray spectroscopy) system in hypermode. X-ray photoelectron spectra (XPS) measurements were taken on a Sigma 2 spectrometer (Thermo Scientific) using a polychromatic Al Kα X-ray source, where binding energy was calibrated taking C 1s = 284.8 eV. For ex-situ XPS analysis, all the electrodes were thoroughly rinsed with dimethyl carbonate in the glove box prior to the measurements. The obtained wet electrodes were naturally dried at room temperature in the glove box before being quickly transferred to the XPS preparation chamber to minimize their contact with air.

For the atomic force microscopy (AFM) measurements we used a Cypher Atomic Force Microscope. N_2 gas sorption measurements were performed on a Quantachrome Autosorb iQ at 77 K. The samples were outgassed at 80°C for at least 12 h before the measurements. The surface area was evaluated by the Brunauer-Emmett-Teller (BET) method and the pore size distribution was determined by a density functional theory (DFT) analysis using a nonlocal DFT (NLDFT) calculation model for nitrogen at 77 K based on cylindrical pores in silica. Thermogravimetric (TGA) analysis was done on a Mettler Toledo TGA/SDTA851^e instrument.

Electrochemical measurements. In a typical preparation of the working electrodes (NVO@rGO and N-rGO), 70 wt% of the active materials were mixed with 20 wt% of carbon black (Super P, TIMCAL) and 10wt% of polyvinylidene fluoride (average Mw ~534000, Aldrich-Fine) in N-methyl-2-pyrrolidinone (99%, Aldrich) through ball milling at a frequency of 20 Hz (concentration of the active material is 12.5 mg/mL). The slurries were transferred onto a titanium current collector and dried in a vacuum oven at 80°C overnight. The typical mass loading of the active materials was ~1.0-1.5 mg cm^{-2}. For half-cell tests, cells were assembled into two-electrode Swagelok-type cells with lithium metal working as both counter and reference electrode. The cell assembly was conducted in an argon-filled glove box. Glass fibers were employed as the separators and 1 M $LiPF_6$ in a 1:1 (v:v) mixture of ethylene carbonate/dimethyl carbonate was used as the electrolyte. For LIB full cells assembly, both the cathode of NVO@rGO and the anode of N-rGO were activated beforehand, during which the electrodes were pre-cycled in half cells for 5 times at the same current density of 150 mA g^{-1}. Afterwards, the cathode was charged to 4.3 V and the anode discharged to 0.01 V to match the capacity between the anode and the cathode. LIB full cells were then assembled with the activated NVO@rGO and N-rGO as the cathode and the anode, respectively. The typical weight ratio between the active materials of the cathode and anode is ~1:1. The electrolyte and the separator applied in the full cells were the same as in the half cells. All electrochemical measurements were performed on a Biologic instrument (VMP3) at room temperature. The EIS measurements were carried out under the frequency range from 100 kHz to 10 mHz. The sinus amplitude was set to 10 mV and the direct current (DC) potential was set to the open-circuit voltage (OCV). The current rates, energy densities, and power densities are based on the total mass of the active materials of both cathode and anode. The energy density and power density are calculated using the following formulas:

$$E = \frac{\int_{t_1}^{t_2} I \times V(t)dt}{3.6m} \tag{1}$$

$$P = \frac{3600E}{\Delta t} \tag{2}$$

where E [Wh kg^{-1}] and P [W kg^{-1}] correspond to the energy and power density, respectively. t_1 [s] and t_2 [s] are the start and end-of-discharge time, respectively. I [A], $V(t)$ [V], m [g] and Δt [s] denote the discharge current, discharge voltage excluding the IR drop, total mass of the active materials (cathode and anode) and discharge time, respectively.

Operando XRD measurements: Operando XRD measurements were carried out on a PANalytical Empyrean diffractometer equipped with a Cu Kα X-ray tube (45 kV, 40 mA) using an in-house-built cell (see Fig. S21). The pattern collection time is around 15 min per scan (step size: 0.0263°/min). During the measurement, the cells were cycled at a constant current rate of 50 mA g^{-1}.

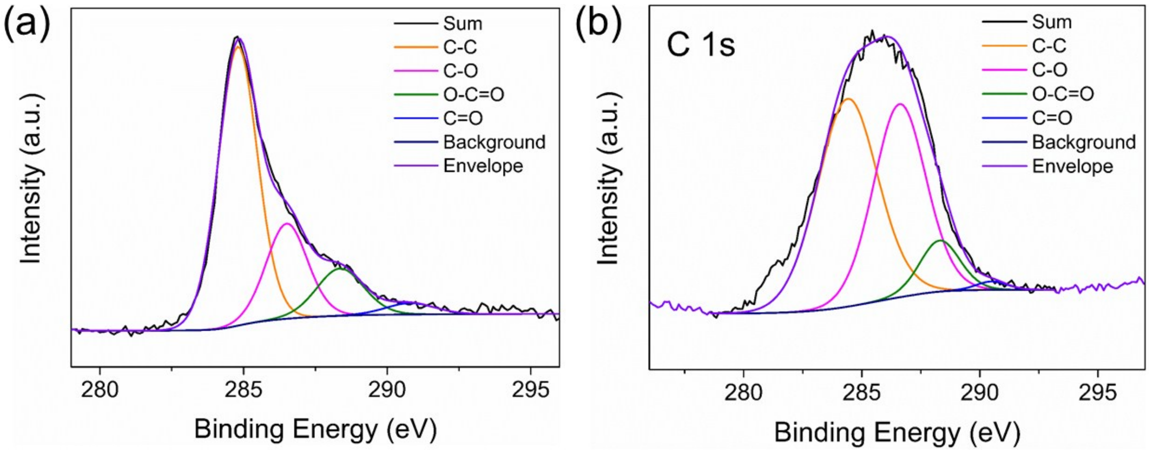

Fig. S1 (a) High-resolution XPS spectra of C 1s for NVO@rGO and (b) the pristine GO.

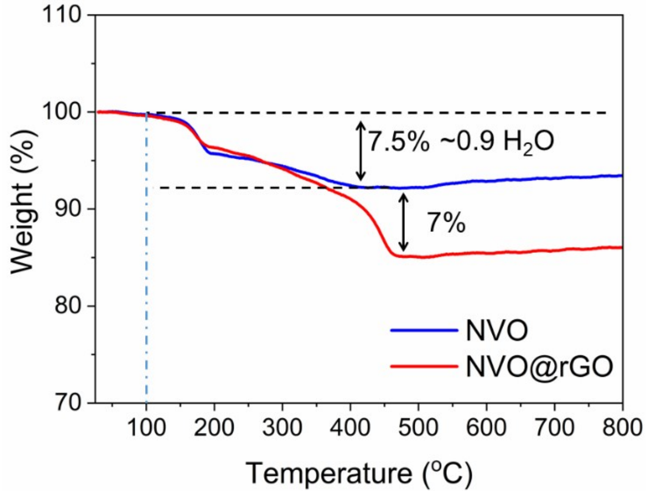

Fig. S2 TGA curves of NVO and NVO@rGO.

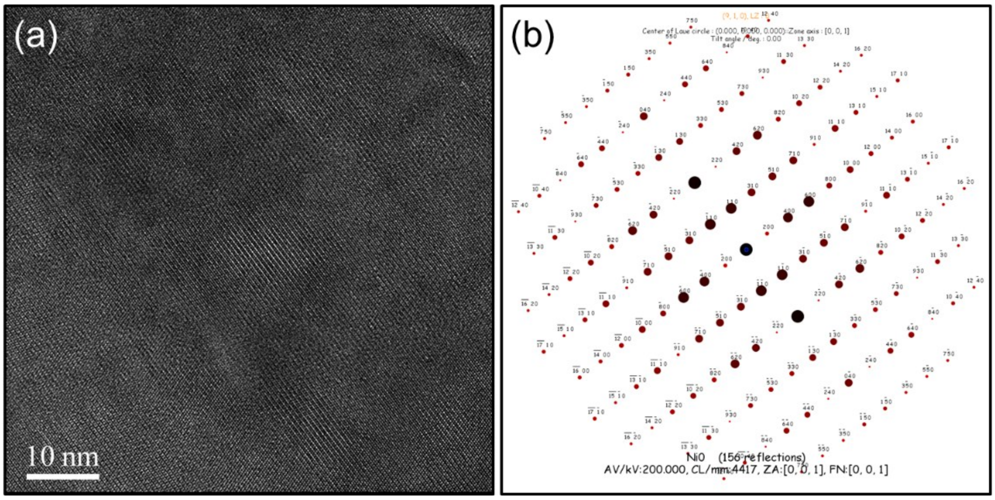

Fig. S3 (a) HRTEM image of NVO. (b) Simulated diffraction pattern of the $Ni_{0.25}V_2O_5{\cdot}nH_2O$ phase using JEMS software.

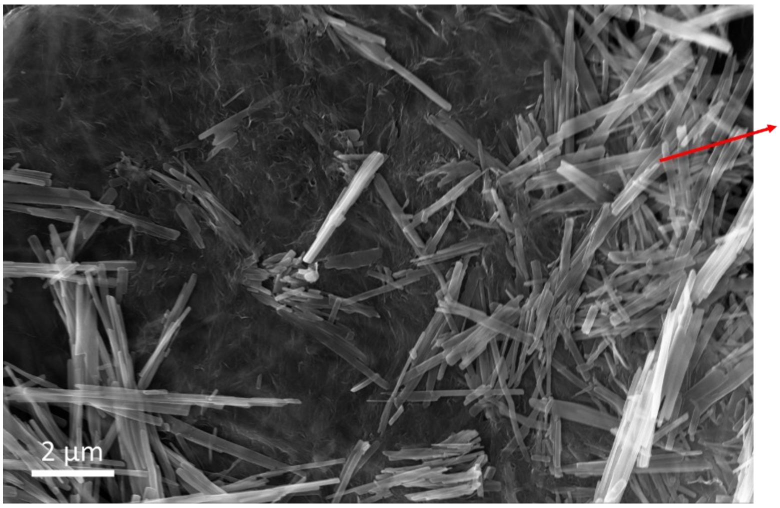

Some NVO nanobelts are not closely connected with the rGO sheets

Fig. S4 SEM overview image of NVO@rGO with NVO nanobelts well embedded in the rGO network and with NVO nanobelts less closely connected to the rGO sheets.

Fig. S5 Photograph of a monolithic N-rGO foam on a dandelion flower, illustrating the low density of the foam.

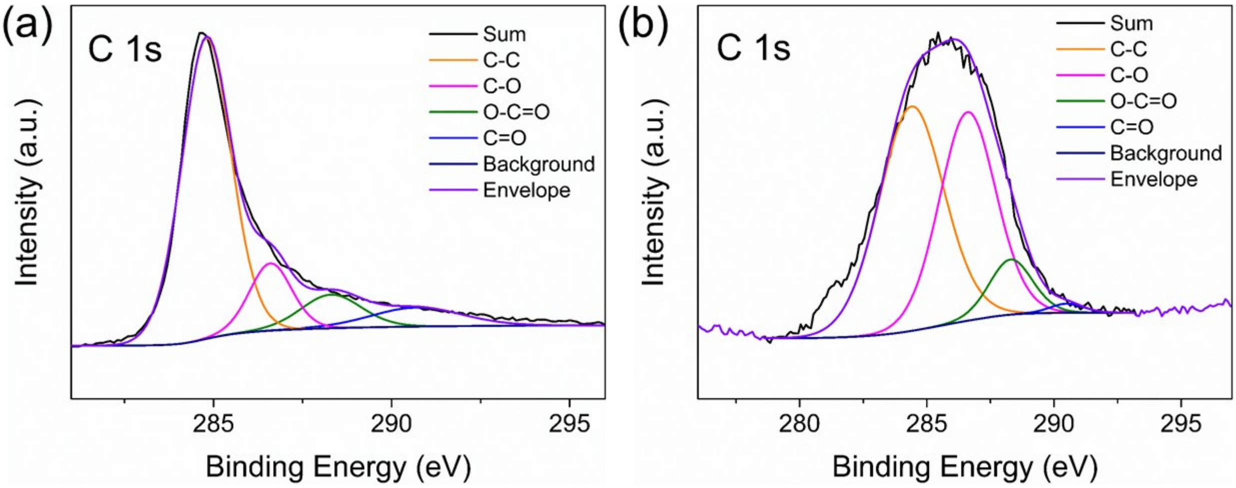

Fig. S6 High-resolution XPS spectra of C 1s for (a) the N-rGO and (b) the pristine GO.

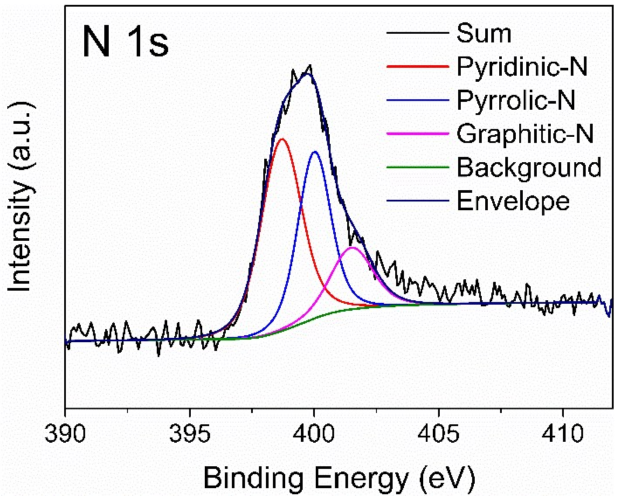

Fig. S7 High-resolution N1s XPS spectrum of N-rGO.

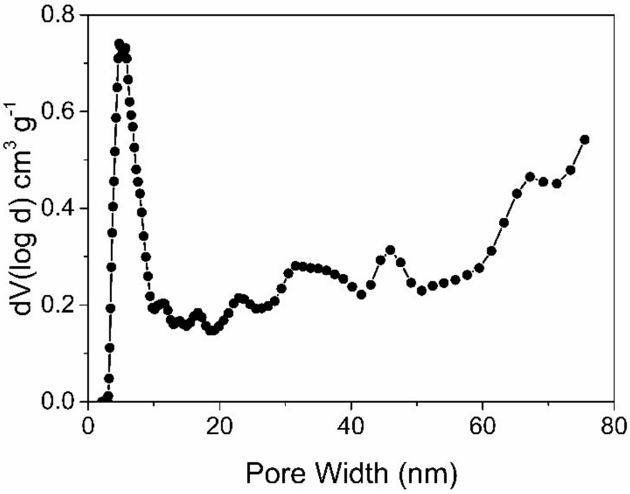

Fig. S8 Pore size distribution obtained by a density functional theory (DFT) analysis for N-rGO.

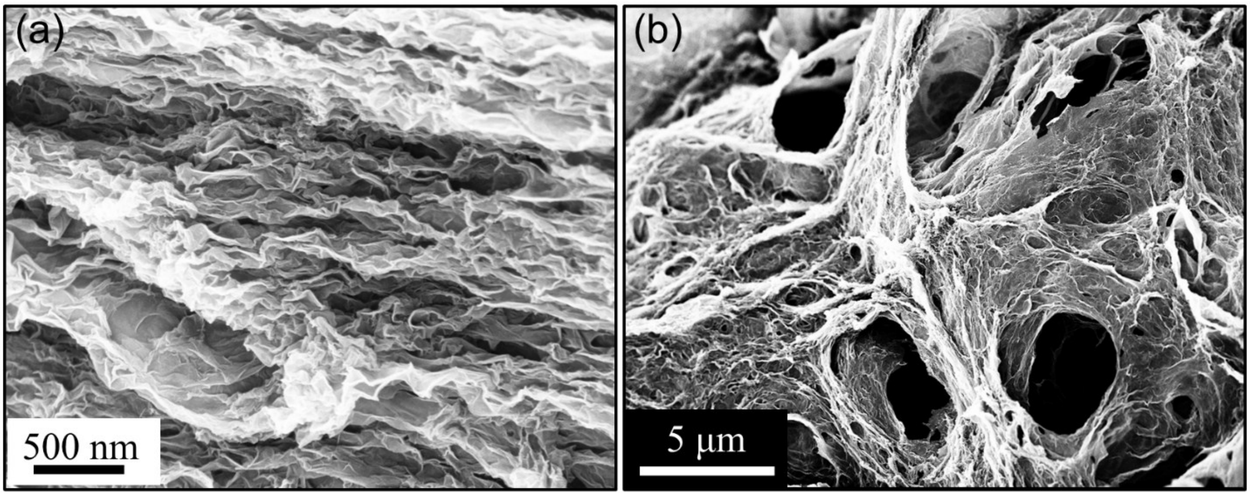

Fig. S9 SEM image of the N-rGO foam at (a) high and (b) low magnification.

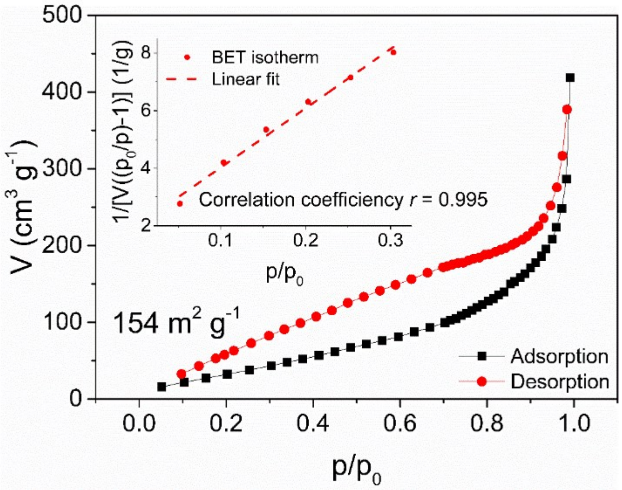

Fig. S10 Complete N_2 adsorption/desorption isotherms of the N-rGO foam (inset: corresponding BET isotherm and linear fit).

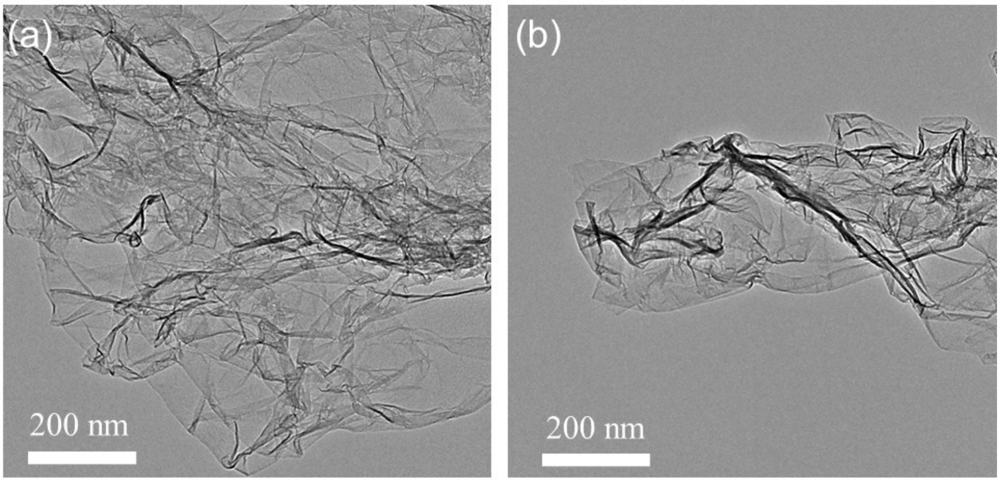

Fig. S11 TEM images of the N-rGO.

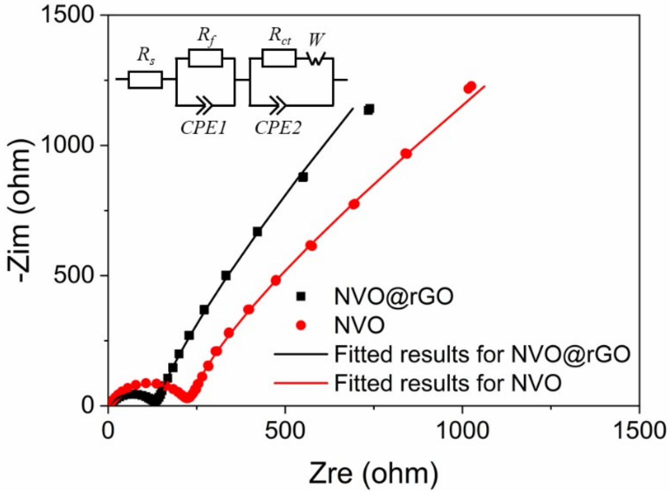

Fig. S12 Original (dots) and fitted (solid lines) EIS results of NVO@rGO and NVO (inset: the equivalent circuit used to fit the EIS).

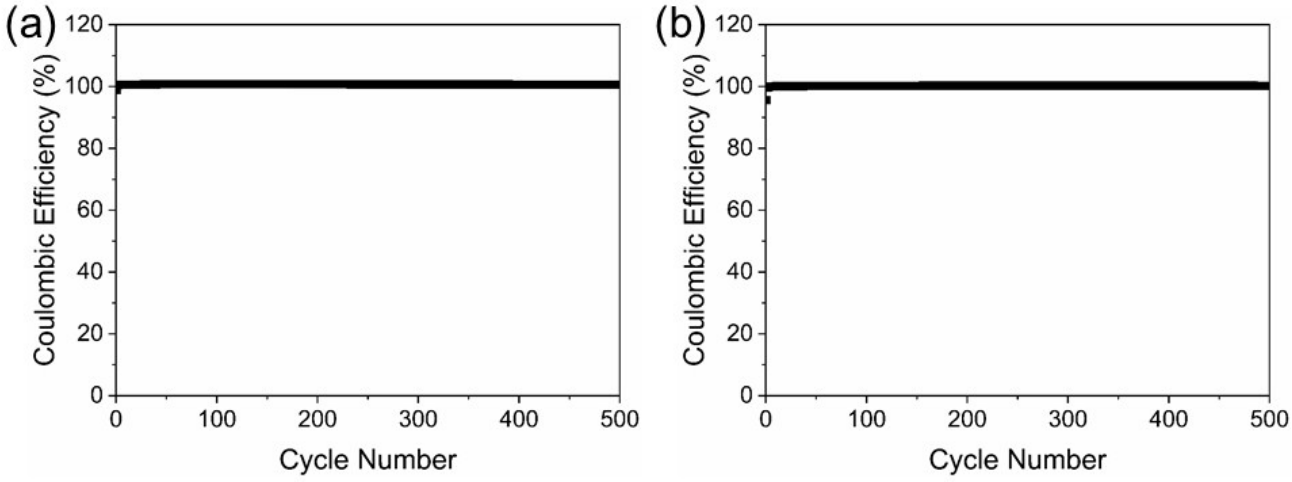

Fig. S13 Coulombic efficiency for NVO@rGO cycled at (a) 15 C and (b) 50 C.

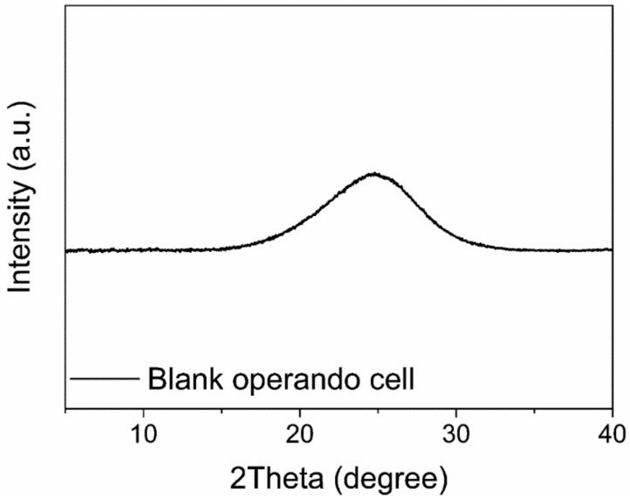

Fig. S14 XRD pattern of the blank operando cell.

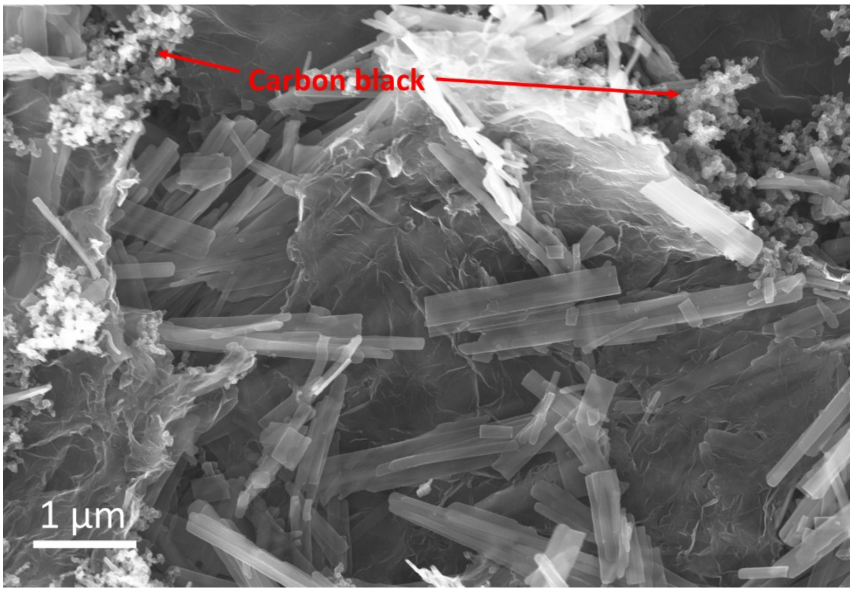

Fig. S15 SEM image of the NVO@rGO electrode after cycling at 15C for 250 cycles.

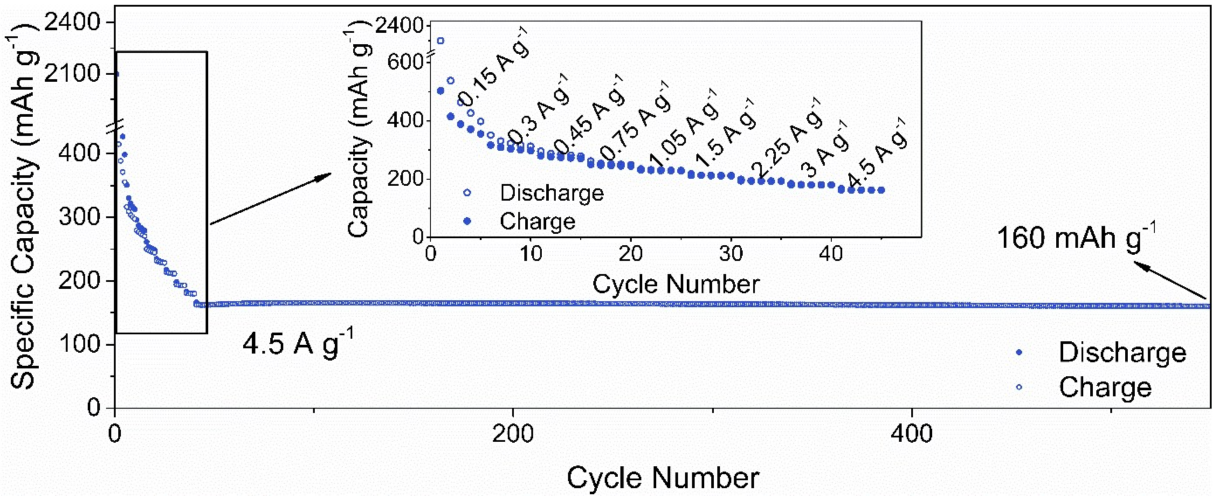

Fig. S16 Cycling performance of the N-rGO foam after a rate capability test. Inset: Magnification of the rate performance test at various current densities.

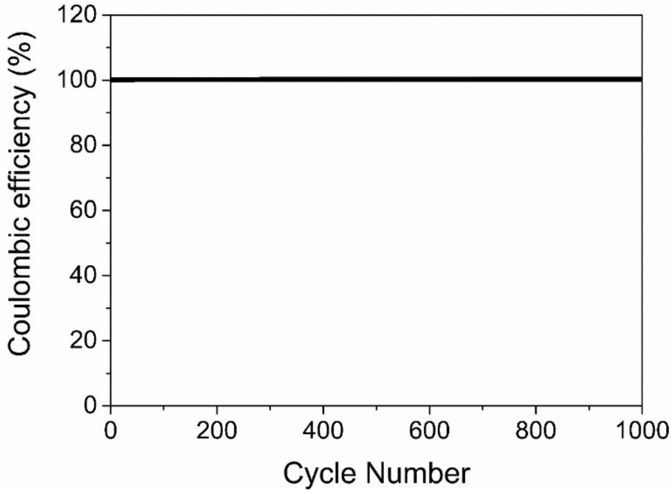

Fig. S17 Coulombic efficiency for N-rGO during cycling at 4.5 A g^{-1}.

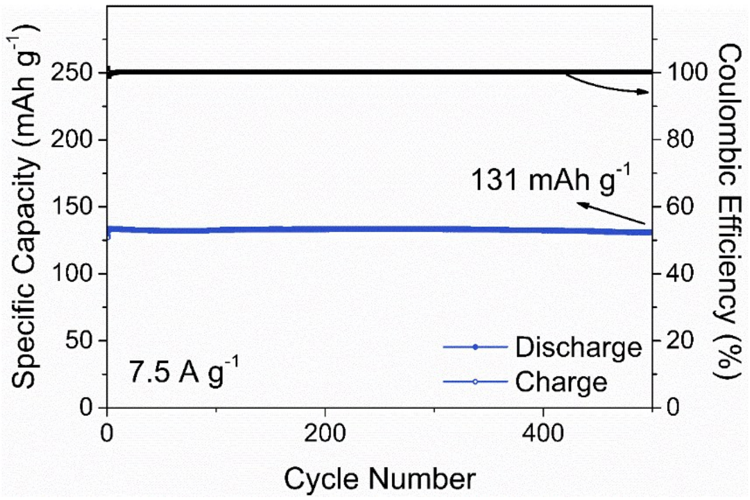

Fig. S18 Cycling performance of N-rGO at a current density of 7.5 A g^{-1}.

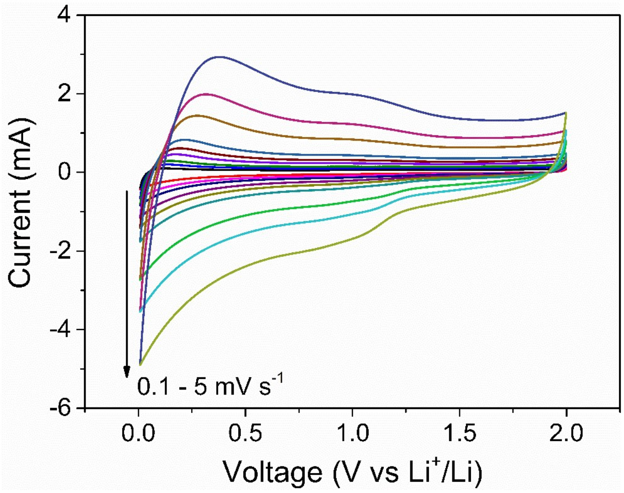

Fig. S19 CV curves of N-rGO at 0.1-5 mV s^{-1}.

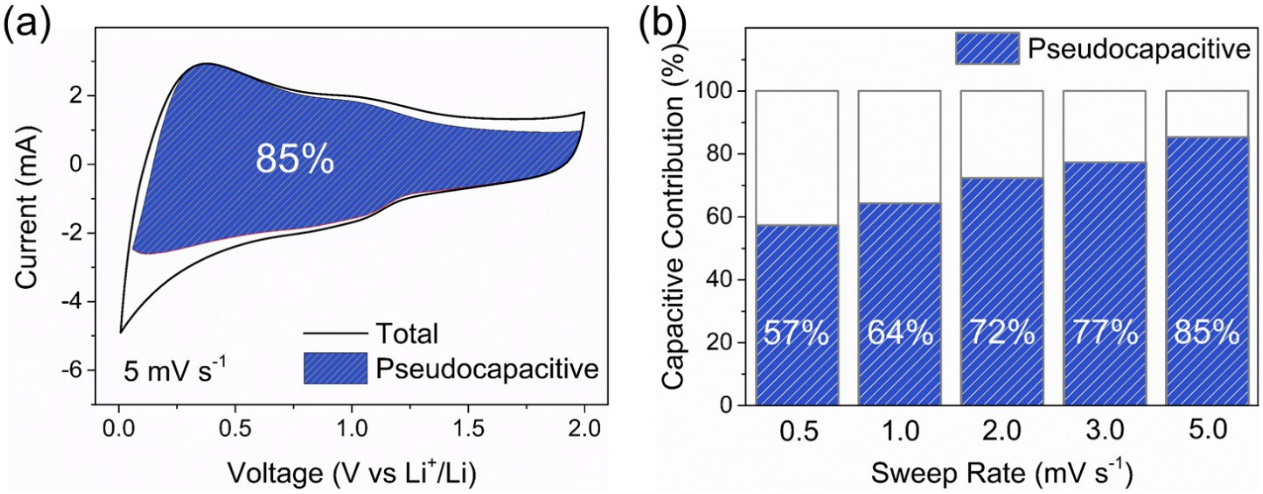

Fig. S20 (a) Voltammetric response of the N-rGO foam separated into the total current (solid line) and the current contributed by pseudocapacitance (shaded area) at a sweep rate of 5 mV s^{-1}. (b) Pseudocapacitive contributions to the total capacity of the N-rGO foam at various sweep rates.

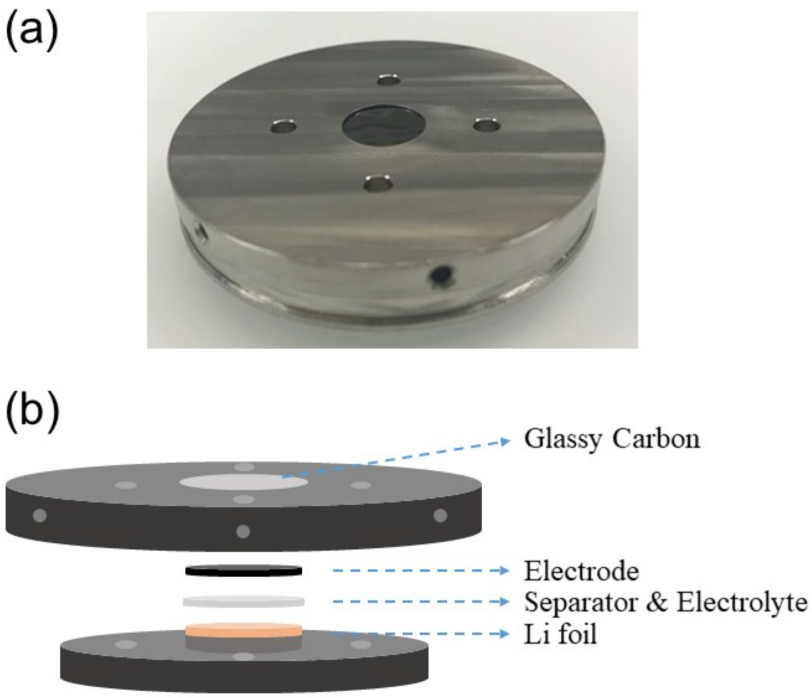

Fig. S21 (a) Photograph and (b) schematic of the in-house-built operando cell.

Table S1 Quantitative analysis of the atomic content of Ni and V in the nickel vanadate nanobelts based on energy dispersive spectroscopy (EDS) analyses.

Element	Series	Norm. at. %
Ni	K-series	11.68511
V	K-series	88.31489

Table S2 Cycling performance comparison of N-rGO || NVO@rGO and some advanced LIB full cells reported in the literature.

Full cells	Reference	Cycles	Current rate	Capacity retention
CNT–Si composite||Li[$Ni_{0.85}Co_{0.05}Mn_{0.10}$]$O_2$	Ref. 3	500	200 mA g^{-1} (based on the total mass)	81%
Graphene || $LiFePO_4$	Ref. 4	80	170 mA g^{-1} (based on the mass of the cathode)	~84%
TiO_2-MoO_3 || $LiCoO_2$	Ref. 5	100	50 mA g^{-1} (based on the total mass)	~64%
Silicon-nanolayer-embedded graphite/carbon hybrids || lithium cobalt oxide	Ref. 6	100	Discharging at 1C and charging at 0.5C	92%
Ge/$LiCoO_2$	Ref. 7	100	500 mA g^{-1} (based on the mass of the anode)	51%
Graphite || lithium polyacrylate-$LiNi_{0.5}Mn_{1.5}O_4$	Ref. 8	80	0.5C	90%
Cu@Si@Cu || $LiFePO_4$	Ref. 9	150	1C	72.4
Graphene ball || $LiNi_{0.6}Co_{0.1}Mn_{0.3}O_2$ coated with graphene ball	Ref. 10	500	5C	88%
Fe-Cu-Si || $LiCoO_2$	Ref. 11	300	1C	63.9%
α-MnS in N,S-codoped carbon || $LiFePO_4$	Ref. 12	100	0.4C	82%
Porous Si/C-graphite || $Li(Ni_{1/3}Mn_{1/3}Co_{1/3})O_2$	Ref. 13	300	Charging at 0.5 mA cm^{-2} and discharging at 0.75 mA cm^{-2}	83%
N-rGO || NVO@rGO	This work	5000	5 A g^{-1} (based on the total mass)	82% (Values refer to capacity retention rather than energy retention)

References

1 L. Sun, Wang L., Tian C., Tan T., Xie Y., Shi K., Li M., and Fu H., *RSC Adv.*, 2012, **2**, 4498-4506.

2 H.-L. Guo, Su P., Kang X., and Ning S.-K., *J. Mater. Chem. A*, 2013, **1**, 2248-2255.

3 J. H. Lee, Yoon C. S., Hwang J.-Y., Kim S.-J., Maglia F., Lamp P., Myung S.-T., and Sun Y.-K., *Energy Environ. Sci.*, 2016, **9**, 2152-2158.

4 J. Hassoun, Bonaccorso F., Agostini M., Angelucci M., Betti M. G., Cingolani R., Gemmi M., Mariani C., Panero S., and Pellegrini V., *Nano Lett.*, 2014, **14**, 4901-4906.

5 C. Wang, Wu L., Wang H., Zuo W., Li Y., and Liu J., *Adv. Funct. Mater.*, 2015, **25**, 3524-3533.

6 M. Ko, Chae S., Ma J., Kim N., Lee H.-W., Cui Y., and Cho J., Nat. Energy, 2016, **1**, 16113.

7 X. Li, Yang Z., Fu Y., Qiao L., Li D., Yue H., and He D., *ACS Nano*, 2015, **9**, 1858-1867.

8 N. P. Pieczonka, Borgel V., Ziv B., Leifer N., Dargel V., Aurbach D., Kim J. H., Liu Z., Huang X., and Krachkovskiy S. A., *Adv. Energy Mater.*, 2015, **5**, 1501008.

9 Z. Zhang, Wang Z. L., and Lu X., *ACS Nano*, 2018, **12**, 3587-3599.

10 I. H. Son, Park J. H., Park S., Park K., Han S., Shin J., Doo S.-G., Hwang Y., Chang H., and Choi J. W., *Nat. Commun.*, 2017, **8**, 1561.

11 S. Chae, Ko M., Park S., Kim N., Ma J., and Cho J., *Energy Environ. Sci.*, 2016, **9**, 1251-1257.

12 D. H. Liu, Li W. H., Zheng Y. P., Cui Z., Yan X., Liu D. S., Wang J., Zhang Y., Lü H. Y., and Bai F. Y., *Adv. Mater.*, 2018, **30**, 1706317.

13 X. Li, Yan P., Xiao X., Woo J. H., Wang C., Liu J., and Zhang J.-G., *Energy Environ. Sci.*, 2017, **10**, 1427-1434.